Journal of Power Sources 196 (2011) 7188–7194

Contents lists available at ScienceDirect

Journal of Power Sources

journal homepage: www.elsevier.com/locate/jpowsour

H_2O chemisorption and H_2 oxidation on yttria-stabilized zirconia: Density functional theory and temperature-programmed desorption studies

Alexandr Gorski*, Vitaliy Yurkiv, Dzmitry Starukhin, Hans-Robert Volpp

Heidelberg University, Institute of Physical Chemistry, Im Neuenheimer Feld 229, 69120 Heidelberg, Germany

ARTICLE INFO

Article history:
Received 15 June 2010
Received in revised form
16 September 2010
Accepted 29 September 2010
Available online 7 October 2010

Keywords:
Solid oxide fuel cell
Hydrogen oxidation
Elementary kinetic modeling
Temperature programmed desorption
Density functional theory

ABSTRACT

The mechanism of H_2O dissociation as well as the adsorption and oxidation reaction of H_2 on yttria-stabilized zirconia (YSZ), commonly used as part of solid oxide fuel cell (SOFC) anodes, was investigated employing temperature-programmed desorption (TPD) spectroscopy and density functional theory (DFT). In agreement with theory the experimental results show that interaction of gaseous H_2O with YSZ results in dissociative adsorption leading to strongly bound OH surface species. In the interaction of gaseous H_2 with an oxygen-enriched YSZ surface (YSZ + O) similar OH surface species are formed as reaction intermediates in the H_2 oxidation. Our experiments showed that in both the H_2O/YSZ and the H_2/YSZ + O heterogeneous reaction systems noticeable amounts of H_2O are "dissolved" in the bulk as interstitial hydrogen and hydroxyl species. The experimental H_2O desorption data is used to access the accuracy of the H_2/H_2O/YSZ adsorption/desorption and surface reaction kinetics data, employed in previous modeling studies of the electrochemical H_2 oxidation on Ni-pattern/YSZ model anodes by Vogler et al. [J. Electrochem. Soc., 156 (2009) B663] and Goodwin et al. [J. Electrochem. Soc., 156 (2009) B1004]. Finally a refined experimentally validated H_2/H_2O/YSZ adsorption/desorption and surface reaction kinetics data set is presented.

1. Introduction

Among the different types of fuel cells, all of which convert chemical energy of a fuel gas directly into electrical energy, solid oxide fuel cells (SOFCs) possess the highest electrical efficiency. Furthermore for SOFCs, as compared to conventional fuel combustion concepts such as internal combustion engines and turbines, the emission of e.g. nitrogen oxides (NO_x) is only marginal. Hence, SOFCs are widely regarded as environmentally friendly energy sources (see e.g. [1,2] and references therein). In addition, if operated in the reverse mode as solid oxide electrolysis cells (SOECs) they can be used to store electrical power at times of electricity over-plus [3]. However, although the traditional nickel (Ni)/yttria-stabilized zirconia (YSZ) anode material combination is widely used in SOFCs, the actual microscopic details of the electrochemical reaction mechanism occurring at the three-phase boundary (TPB) of gas-phase, electrode, and electrolyte, are not yet fully understood even for systems as simple as the electrochemical oxidation of hydrogen (H_2), which can be described by the global reaction $H_{2(g)} + O^{2-}{}_{YSZ} \rightarrow H_2O_{(g)} + 2e^-{}_{Ni}$, and the electrochemical reduction of water, $H_2O_{(g)} + 2e^-{}_{Ni} \rightarrow H_{2(g)} + O^{2-}{}_{YSZ}$, respectively. The latter one being important if the cell is operated as SOEC.

The elucidation of the surface reaction mechanisms underlying these two global charge transfer reactions is considered as one of the most difficult aspects of understanding the fundamental electrochemical behavior of SOFCs [2]. As outlined in a recent review article by Sun and Stimming [4] a detailed understanding of the anode charge transfer reaction mechanisms and kinetics plays a vital role in the systematic development and optimization of advanced SOFC anode materials. In recent years numerical simulations based on computational reaction–diffusion models, which explicitly consider the coupled behavior of reagent/product adsorption/desorption and diffusion, elementary thermal surface reactions and elementary charge transfer reaction steps, have emerged as valuable tools to shed light on the electrochemical reaction processes even for complex geometries of ceramic–metallic composite anodes generally employed for SOFCs [5]. If the aim is on the determination of quantitative elementary reaction kinetics information about the TPB electrochemistry, however, numerical simulations of electrochemical characterization measurements (such as polarization and impedance data) of model anode systems with simplified and well characterized TPB geometries – such as patterned and point electrodes – are required. At this point it should be noted, however, that the reliability of the charge transfer reaction kinetics data derived with this approach strongly depends on the employed electrode kinetics model and the accuracy of the respective elementary surface reaction kinetics data set.

* Corresponding author. Tel.: +49 6221 54 5013, fax: +49 6221 54 5050.
E-mail address: alexandr.gorski@pci.uni-heidelberg.de (A. Gorski).

0378-7753/$ – see front matter © 2010 Elsevier B.V. All rights reserved.
doi:10.1016/j.jpowsour.2010.09.090

Various H_2/H_2O/Ni-YSZ electrode kinetics models have been reviewed in [4]. In addition, a critical summary of the H_2/H_2O/Ni-YSZ electrode kinetics models as used in different kinds of numerical simulation approaches of experimental SOFC anode data can be found in [6]. As outlined in [4], the available electrode kinetics models mainly disagree with regard to the actual location where – either mainly on the Ni [7] or both on the Ni and on the YSZ surface [8,9] – the heterogeneous chemical and electrochemical elementary reaction steps take place. As noted in [6], the contribution of the reaction of H_2 with $O^{2-}{}_{YSZ}$ directly on the YSZ surface – followed by electron migration to Ni through the YSZ – was suggested in Refs. [10,11]. The formation of interstitial hydrogen and hydroxyl at the Ni electrode/YSZ electrolyte two phase boundary was proposed in Refs. [12,13]. The partial contribution of water production and dissociation through the formation of OH surface species on YSZ was put forward in Refs. [8,9]. Also, as have been shown by Sakai et al. the effect of water dissolution in ceria–zirconia–yttria polycrystals may influence significantly the surface exchange rate constant [14].

Based on experimental electrochemical data obtained for well-defined Ni-pattern/YSZ model anodes, which revealed that the presence of H_2O in the fuel gas has a "catalytic" effect on the anode kinetics, a mechanism (similar to the one previously proposed in Ref. [15]) was suggested where the presence of OH on the YSZ surface would allow for an efficient proton migration on the YSZ (towards the Ni electrode) resulting in an effective enlargement of the electrochemical active region for the anode kinetics [16]. In a "Space-state modeling" analysis of the latter experimental data, however, due to the lack of quantitative adsorption and reaction kinetics data for H and OH on YSZ, the authors employed a mechanism where the heterogeneous reactions involving H, OH, and H_2O take place solely on the Ni surface [17]. As a consequence, however, the proposed YSZ mediated catalytic effect of H_2O could not be investigated in the framework of this modeling work.

In a subsequent more detailed analysis of the Ni-pattern/YSZ model anode data of Ref. [16], which was based on an elementary kinetics surface reaction-diffusion model, the adsorption and dissociation reactions of H_2O on the YSZ surface were included [18]. A sensitivity analysis performed in the course of the latter study clearly emphasized the great influence of the thermodynamic and reaction kinetics data of YSZ surface species on the electrochemical modeling results (see e.g. Fig. 5 of Ref. [18]). A similar surface reaction–diffusion model based computational approach was applied in Ref. [19] to analyze Ni-pattern/YSZ model anode data reported in Refs. [20,21]. The surface reaction mechanism of Ref. [19] included the adsorption and dissociation reactions of H_2O as well as H_2O formation due to H_2 oxidation on the YSZ electrolyte surface. In both computational studies [18,19], good agreement with the respective experimental target data [16,20,21], could be achieved, although the H_2O/YSZ adsorption/dissociation and surface reaction kinetics data were considerably different. While the data employed in [18] was based on estimates partially guided by results of quantum chemical calculations of H_2O dissociation on TiO_2 [22], the kinetics data of [19] was derived by the authors from a sophisticated computational modeling of a thermogravimetrical data set reported in Fig. 17 of Ref. [15]. In the light of the importance the H_2/H_2O/YSZ surface kinetics data play in the reaction mechanisms employed in the computational studies of Ni-pattern/YSZ model anode data [18,19], further studies are desirable, the results of which allow for a validation and, if necessary, the refinement of the employed H_2/H_2O/YSZ kinetics data sets. Experimentally validated kinetics data would also allow to assess in more detail both the accelerating effect of H_2O on SOFC performance as well as the validity of the assumption underlying the computational approaches, namely that the charge transfer reaction(s) are the main rate limiting steps (for further details see [6] and references therein).

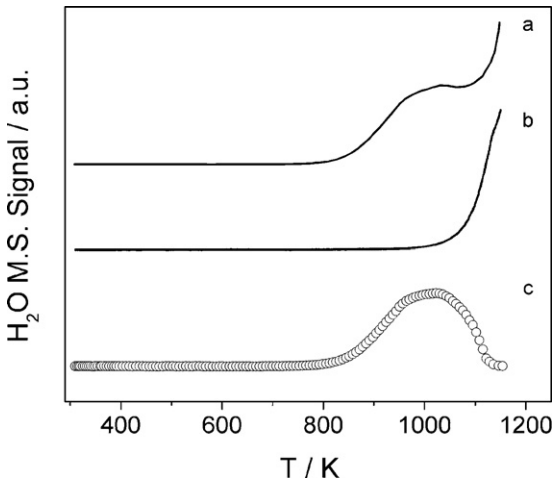

Fig. 1. Schematic illustration of the background subtraction procedure applied to account for H_2O MS signal contributions due to H_2O desorbing from the sample holder. Curve a: Raw H_2O TPD spectrum. Curve b: Background contribution from the sample holder. Curve c: Background subtracted TPD spectrum representing H_2O desorbing from the YSZ sample. The TPD spectra are shifted vertically against each other for ease of clarity.

In the following results of temperature-programmed desorption (TPD) of H_2O dissociation/desorption and H_2 oxidation over YSZ will be presented, which allow for a direction comparison with simulated TPD spectra based on the H_2/H_2O/YSZ surface kinetics data sets of Refs. [18,19], respectively. In addition, following the approach of Ref. [23], quantum chemical calculations based on density functional theory (DFT) were performed, to investigate the molecular energetics of H_2O adsorption/dissociation and H_2 oxidation on YSZ.

2. Experimental methodology

The TPD studies of H_2O desorption and H_2 oxidation on YSZ were performed in a vacuum chamber (base pressure 10^{-9} mbar), which has been used previously to investigate CO desorption and oxidation on Pt, Rh, Ni and YSZ surfaces (for further details see [24] and references therein). The chamber was pumped by a turbo pump backed by a Roots pumping station. It was equipped with a quadrupole mass spectrometer (QMS) for TPD measurements, and a retarding field analyzer for low-energy-electron diffraction (LEED) studies. In the present work polycrystalline YSZ sample plates (8.5% mol Y_2O_3) with a thickness of 0.2 mm were employed. The original YSZ sample plate was obtained from Itochu (Tokyo, Japan). The temperature of the YSZ samples could be varied from 300 K up to 1200 K. The substrate temperature was measured by a thermocouple attached to the sample surface.

Different kinds of H_2O TPD measurements were performed in the course of the present work. In a first series of H_2O TPD experiments YSZ samples exposed to ambient air humidity ($p(H_2O) \approx 24$ mbar) were introduced into the vacuum chamber and flashed to a temperature of 700 K in order to desorb impurities and physisorbed H_2O from the YSZ sample surface. After cooling down to 300 K the actual desorption spectrum was obtained by recording the H_2O mass spectrometer (MS) signal while the sample was heated from 300 K to ca. 1200 K with a linear heating rate of 1 K s^{-1}. A typical raw experimental TPD spectrum is shown in the upper part of Fig. 1 as curve a. In order to obtain a TPD spectrum representing the actual desorption of H_2O from the YSZ sample the H_2O signal background originating from sample holder parts (curve b in Fig. 1), which are heated up with some time delay, had to be subtracted. The background corrected TPD spec-

trum originating solely from H_2O molecules desorbing from the YSZ sample is depicted as curve c in Fig. 1. All TPD spectra shown in the following were obtained by applying this background correction procedure.

3. Quantum chemical calculations

Quantum chemical calculations based on density functional theory (DFT) were performed to investigate H_2 oxidation and H_2O dissociation energetics on YSZ surfaces. As in our previous DFT studies [25] the present calculations were performed using the CASTEP (Cambridge Sequential Total Energy Package) computer code [26] in the framework of the generalized gradient approximation (GGA), as proposed by Perdew et al. [27], in combination with Vanderbilt ultrasoft pseudopotentials [28]. For systems with an even number of electrons restricted nonspin-polarized calculations were performed. For systems with an odd number of electrons unrestricted spin-polarized calculations were performed. The plane wave basis set was truncated at a kinetic energy of 420 eV. Computations were performed over a range of *k*-points within the Brillouin zone as generated by the full Monkhorst–Pack scheme [29] with a $2 \times 2 \times 1$ mesh. A further increase of the cut off energy and the number of *k*-points resulted in negligibly small changes in adsorption energies (typically less than 5 kJ mol^{-1}), indicating that the energy values are well converged. A slab was repeated periodically, leaving at least a 10 Å wide vacuum region in the direction perpendicular to the surface. The atoms of the bottom multilayer were fixed in all calculations, while the positions of atoms of the two outermost multilayers and the positions of atoms of the adsorbed molecules were optimized during the process of structural relaxation. A complete linear synchronous transit (LST)/quadratic synchronous transit (QST) scheme [30] was used in the transition state searches for the surface reaction steps. A force convergence criterion of 0.03 eV Å^{-1} was applied in all calculations.

The slabs used in the present study to investigate H_2 oxidation on an oxygen-enriched YSZ surface, denoted as YSZ + O in the following, and H_2O dissociation on a YSZ surface are reproduced in Fig. 2(a) and (b), respectively. The procedure applied to obtain a representative slab for the (1 1 1) surface of YSZ as shown in Fig. 2(b) is similar to the one described in Ref. [23], which starts from a pure (1 1 1) terminated zirconia slab, which consists of 12 ZrO_2 formula units with 36 atoms (for further details see Ref. [23] and Fig. 2 therein). From the pure zirconia slab an oxygen atom was removed to account for vacancy formation (denoted as "vac." in Fig. 2(b)) and two zirconium atoms were substituted by two yttrium atoms which are depicted as black atoms (Y) corresponding to a 9% mol concentration of yttria in YSZ. The energetically most stable YSZ slab corresponds to the structure with two atoms of yttrium close to each other and preferentially occupying the next-nearest neighbor sites to the oxygen vacancy [31,32]. Therefore, for calculations, we adopted the mentioned YSZ slab with the subsurface vacancy and two Y atoms, substituting Zr in the outermost and the second surface layers. Finally, in order to generate an oxygen-enriched surface, an additional oxygen atom (marked by * in Fig. 2(a)) was introduced to occupy the subsurface oxygen vacancy of YSZ. The four different surface oxygen atoms of the YSZ + O surface unit cell are indicated by the numbering (i = 1–4).

In Fig. 3 two low energy reaction pathways for the heterogeneous H_2 oxidation reaction on the YSZ + O surface as obtained in the DFT calculations are schematically depicted. Both, the pathway shown in the upper part (I) and the pathway shown in the lower part (II) of Fig. 3 lead to direct formation of gaseous $H_2O_{(g)}$ and YSZ by barrier less dissociative adsorption of H_2 on surface oxygen atoms via the formation of OH surface intermediates, which can further react to yield surface H_2O that finally desorbs into the gas phase leaving back an YSZ surface. The energetics of the two reaction

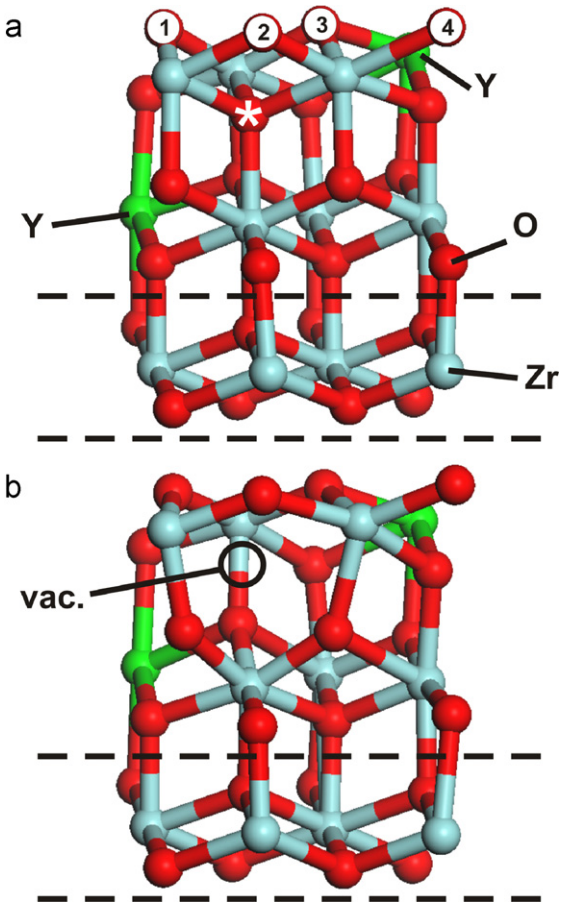

Fig. 2. Slabs employed in the present DFT calculations: (a) Oxygen rich YSZ + O with the additional oxygen atom (*) occupying the subsurface oxygen vacancy of YSZ, the structure of which is reproduced in (b) with the positing of the subsurface oxygen vacancy marked as "vac." For further details see text.

pathways I and II illustrated in Fig. 3 is depicted in Fig. 4(a) and (b), respectively. The latter results also reveal that the reverse reaction namely the dissociative adsorption of H_2O on YSZ leading to surface OH proceeds is an activated process with overall DFT activation energies of E_a(I) = 121.3 kJ mol^{-1} and E_a(II) = 91.4 kJ mol^{-1}. The latter value is in reasonable agreement with the value of 86.8 kJ mol^{-1} in the sticking probably expression used by Goodwin et al. [19] to describe the overall process of dissociative H_2O chemisorption. In the mechanism of Ref. [18], on the other hand, the dissociative chemisorption of H_2O is assumed to occur with considerably lower activation energy of 9.6 kJ mol^{-1}.

At this point we would like to note that we also performed comprehensive DFT calculations to investigate the adsorption of H_2 on the YSZ surface. For this reaction system, however, we were unable to locate any low energy dissociative adsorption pathway resulting in surface OH formation without applying artificial constrains. Our unconstrained DFT calculations showed that the dissociative adsorption of H_2 on YSZ requires an activation energy of at least 200 kJ mol^{-1}. Hence we conclude, in mutual agreement with the DFT results reported in Ref. [23], that in contrast to the interaction of H_2 with a YSZ + O surface the formation of OH surface species as well as any subsequent formation of water due to the interaction of H_2 with YSZ is energetically highly unfavorable.

4. Experimental TPD spectra and simulations

In Fig. 5a "time series" of H_2O TPD spectra obtained for a YSZ sample exposed to ambient air humidity prior to the mea-

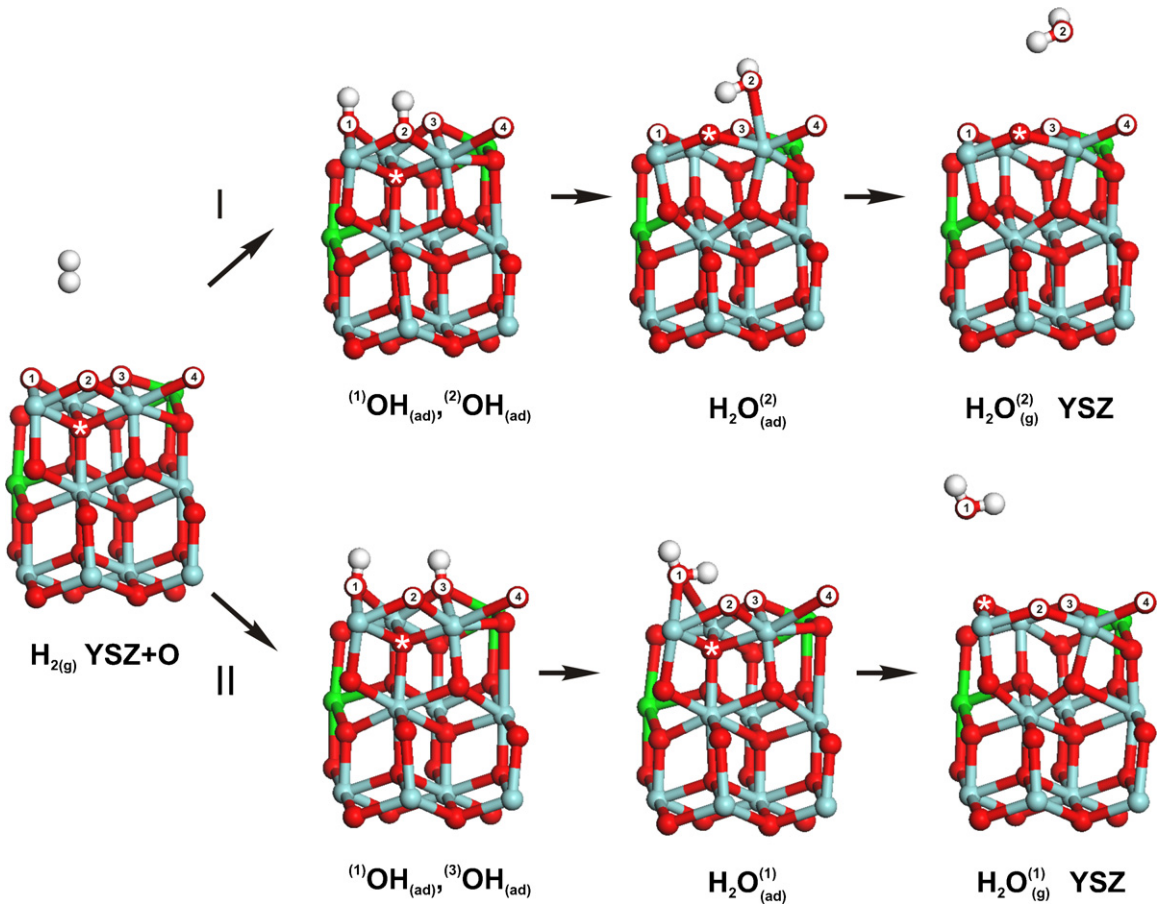

Fig. 3. Illustration of two low energy surface reaction pathways I and II as obtained in the present DFT studies of the heterogeneous H_2 oxidation reaction on the YSZ + O surface. Numbering of the oxygen surface atoms initially present at the YSZ + O surface is the same as in Fig. 2 (a). Further details are given in the text.

surements is depicted. The three consecutively recorded spectra (curves (a)–(c)) revealed the decreasing amount of desorbing H_2O molecules as manifested by curve (c), which was obtained in run three, where practically no H_2O desorption signal could be observed anymore. However, exposing the sample (after curve (c) had been recorded and the sample had been cooled back to ca. 320 K) to a water pressure of 1×10^{-6} mbar for 25 min (corresponding to an exposure of 1100 Langmuir) resulted in a clearly observable H_2O spectrum in the subsequent TPD run (curve (d) in Fig. 5). By comparing the sum of the integrated areas of the two TPD spectra ((a) and (b) in Fig. 5) with the integrated area of a CO TPD spectrum obtained from a platinum (1 1 1) sample—exposed to a partial pressure of 10^{-8} mbar CO until a sharp c(4 × 2)Pt(1 1 1)-CO LEED pattern corresponding to a CO coverage of 0.5 monolayer was observed [33]—a value $x(H_2O_i) = 6 \times 10^{-5}$ could be estimated for the mole fraction of H_2O solved in YSZ. In the latter estimate the different electron impact ionization cross sections of CO (to CO^+ [34]) and H_2O (to H_2O^+ [35]) were taken into account. A value of 15×10^{14} atoms cm^{-2} was used for the Pt(1 1 1) surface atom density along with a YSZ bulk density value of 6.1 g cm^{-3}. Assuming that the solution of H_2O in YSZ leads to the formation of two interstitial protons (hydrogen, H_i) this value corresponds to a value of $x(H_i) = 12 \times 10^{-5}$ for the mole fraction of solute protons. The latter value is approximately five times higher than the value of $x(H_i) = 2.2 \times 10^{-5}$ obtained in Ref. [36] for YSZ (10 mol% Y_2O_3) at comparable H_2O partial pressure of 24 mbar.

In a second set of experiments YSZ samples (after having been flashed at least three times up to 1200 K in order to completely remove the YSZ H_2O contents) were exposed to a H_2/O_2 atmosphere ($p(H_2) = p(O_2) = 1 \times 10^{-6}$ mbar) before H_2O TPD spectra were recorded. The results of these reactive TPD measurements allow for comparison with the results obtained in a numerical simulation of H_2O formation TPD spectra (vide infra) based on the H_2/YSZ oxidation kinetics data used in Ref. [19]. Finally it should be noted that calibration experiments similar to the one performed in the H_2O adsorption/desorption studies described above revealed that YSZ exposure to a H_2/O_2 atmosphere also leads to a considerable amount of YSZ bulk H_2O formation resulting in vales of $x(H_2O_i) = 3.2 \times 10^{-5}$ and $x(H_i) = 6.4 \times 10^{-5}$, respectively, which are only a factor of two lower than the values obtained in the present water adsorption studies.

Numerical simulations of TPD spectra were carried out using the DETCHEM software package [37], which allows the calculation of temperature- and time-dependent surface coverages and surface species fluxes in the framework of a zero-dimensional surface reaction model employing thermodynamically consistent reversible elementary reaction kinetics.

In Fig. 6(a) results of simulations of H_2O TPD spectra obtained using the two different sets of H_2O/YSZ adsorption/desorption and surface reaction kinetics data previously used in the modeling of the electrochemical oxidation data obtained for H_2/H_2O Ni-pattern/YSZ model anode systems in Refs. [16,20,21], respectively. The dash-dotted line was obtained using the surface reaction kinetics data as given in Table III of Ref. [18]. The dashed line was obtained using the reaction kinetics data given in Table IV of Ref. [19]. In each simulation the thermodynamics data as reported in the respective articles was used. For comparison a simulated TPD

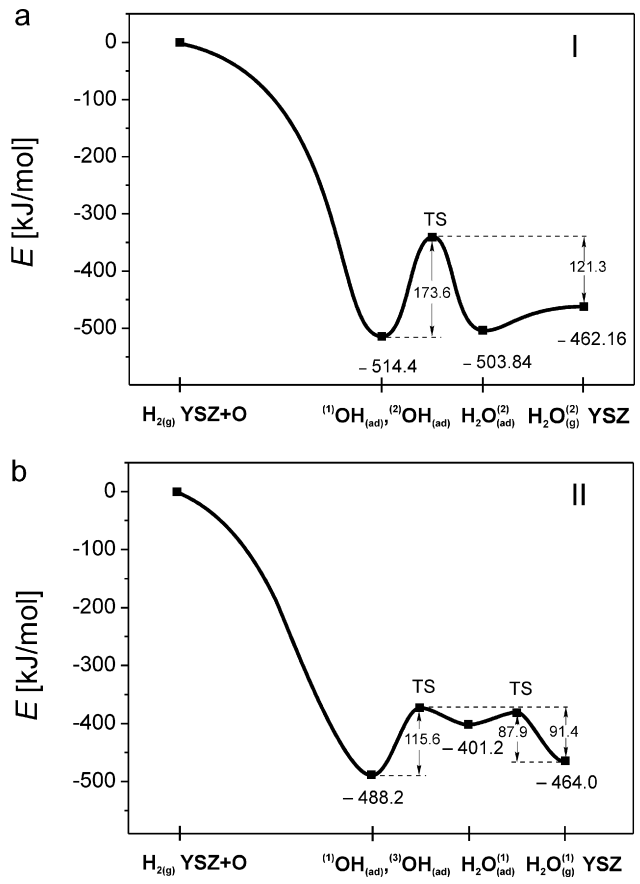

Fig. 4. Energetic pathways for the two surface reactions. The energy pathway depicted in (a) corresponds to the reaction sequence Fig. 3 I. The energy pathway reproduced in (b) corresponds to the reaction sequence Fig. 3 II.

spectrum obtained using refined surface kinetics data as listed in Table I, is depicted as a solid curve. All simulations were performed for a H_2O pressure of 10^{-6} mbar to allow for direct comparison with the experimental spectrum (open symbols in Fig. 6(a)).

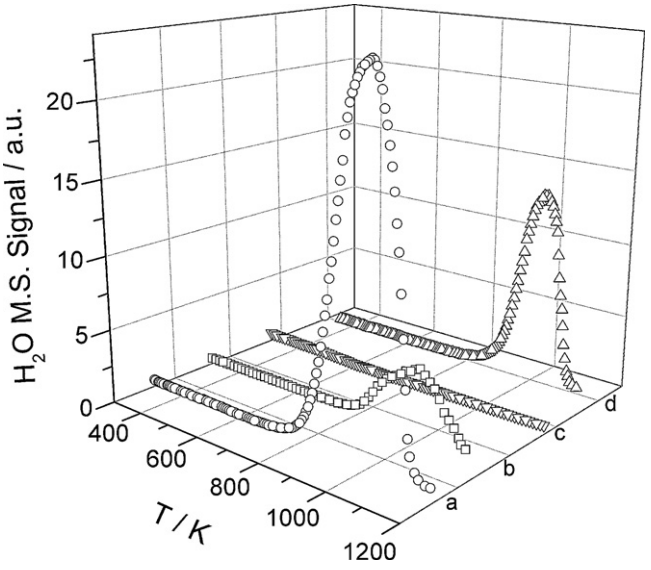

Fig. 5. Series of H_2O TPD spectra. Spectrum a: First spectrum of a YSZ sample exposed to ambient air humidity prior to the TPD measurement. Spectrum b: Second spectrum recorded right after spectrum a. Spectrum c: Third spectrum recorded right after spectrum b. Spectrum d: Recorded after the YSZ sample was exposed to a water pressure of 1×10^{-6} mbar for 25 min. Further details are given in the text.

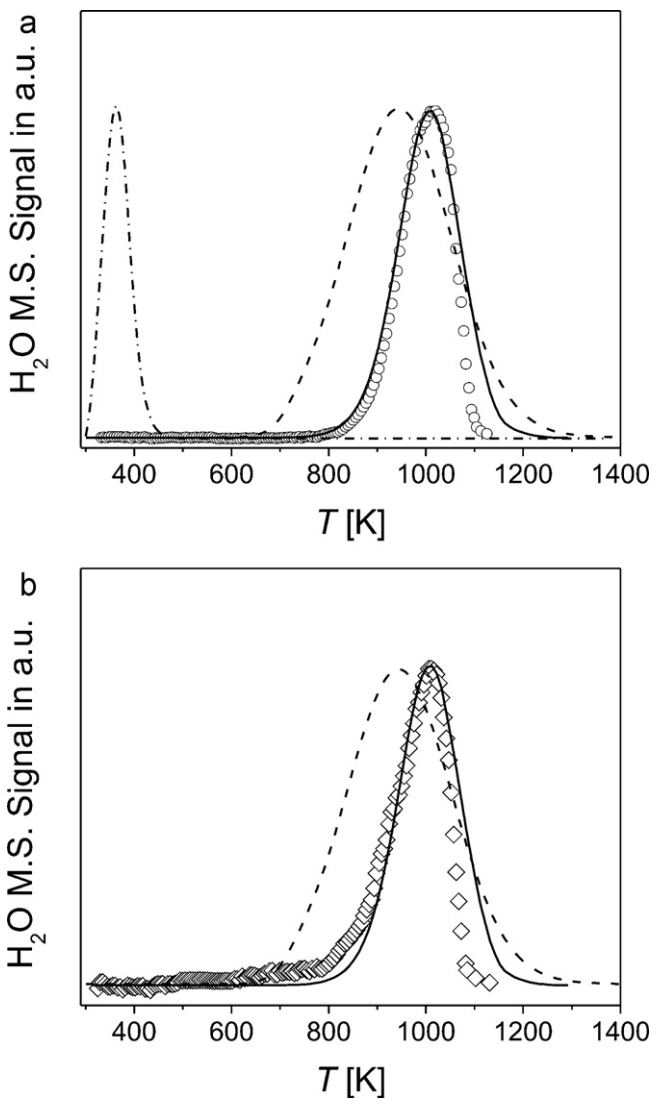

Fig. 6. (a) Comparison of H_2O TPD spectra obtained in numerical simulations based on the adsorption/desorption and surface reaction kinetics data reported in Ref. [18] (dash-dotted curve) and Ref. [19] (dashed curve), respectively, with the corresponding experimental TPD spectrum (open symbols) obtained for a water pressure of 10^{-6} mbar. The solid curve was obtained using the refined mechanism listed in Table 1, which was derived in the present work. (b) Comparison of simulated H_2O TPD spectra obtained using the H_2 oxidation kinetics data (dashed curve) reported in Ref. [19] and the refined kinetics data of Table 1 (solid curve) with the corresponding experimental H_2O spectrum (open symbols) obtained for a H_2/O_2 atmosphere ($p(H_2) = p(O_2) = 1 \times 10^{-6}$ mbar).

Finally in Fig. 6(b) an experimental H_2O TPD spectrum (open symbols) measured in the present H_2 oxidation studies in the presence of a H_2/O_2 atmosphere ($p(H_2) = p(O_2) = 1 \times 10^{-6}$ mbar) is compared with the corresponding theoretical spectrum (dashed curve), which was obtained in a simulation using the H_2 oxidation surface reaction kinetics data of Ref. [19], and with the theoretical spectrum (solid curve), which was obtained using the surface kinetics data given in Table I.

The adsorption/desorption and surface reaction kinetics data set summarized in Table I was obtained in the present work by systematically adjusting the respective pre-exponential factor values (k^0) in the TPD simulation until best agreement with the experimental TPD spectra was achieved. The values for the respective Arrhenius activation energies (E_a) were taken from the DFT calculation results reproduced in Fig. 4(a). The major conceptual difference compared to the mechanism of Ref. [19] is that the present reaction mech-

Table I
Summary of adsorption/desorption and surface reaction kinetics parameters derived from best fit simulations of the present experimental TPD curves.

Reaction		$k^0/s_0^{(*)}$	E_a
$H_2O_{(g)} + []_{YSZ} \rightarrow H_2O_{(ad)}$	(1)	$1.2 \times 10^{-4(*,a)}$	0
$H_2O_{(ad)} \rightarrow H_2O_{(g)} + []_{YSZ}$	(2)	8.5×10^{13} s^{-1}	41.7
$H_2O_{(ad)} + [O]_{YSZ} \rightarrow OH_{(ad)} + OH_{(ad)}$	(3)	1.6×10^{25} cm^2 (mol s)$^{-1}$	164
$OH_{(ad)} + OH_{(ad)} \rightarrow H_2O_{(ad)} + [O]_{YSZ}$	(4)	1.1×10^{17} cm^2 (mol s)$^{-1}$	173.6
$OH_{(ad)} + OH_{(ad)} \rightarrow H_{2(g)} + [O]_{YSZ} + [O]_{YSZ}$	(5)	1.1×10^{10} cm^2 (mol s)$^{-1}$	514.4
$H_{2(g)} + [O]_{YSZ} + [O]_{YSZ} \rightarrow OH_{(ad)} + OH_{(ad)}$	(6)	$1.2 \times 10^{-2(*,b)}$	0

$[]_{YSZ}$: YSZ oxygen surface vacancy; $[O]_{YSZ}$: "oxygen filled" YSZ surface vacancy; E_a: activation energy given in kJ mol^{-1}; k^0: pre-exponential factor; s_0: sticking coefficients. YSZ surface site density is 1.3×10^{-9} mol cm^{-2}.

[*] A sticking coefficient.

[a] From Ref. [38].

[b] From Ref. [19].

anism allows – in agreement with the DFT calculation results – for the existence of surface chemisorbed water, $H_2O_{(ad)}$, which is formed via reaction (1) and which can subsequently dissociate via a thermally activated process (reaction (3)) into surface hydroxyl radicals, $OH_{(ad)}$.

5. Summary and conclusions

The comparison between the H_2O TPD spectra obtained in numerical simulations employing the two different H_2O/YSZ adsorption/desorption and surface reaction kinetics data sets of Ref. [18] (dash-dotted curve in Fig. 6(a)) and Ref. [19] (dashed curve in Fig. 6(a)), respectively, clearly shows that the kinetics data of Goodwin et al. [19] leads to a considerable better agreement with the experimental TPD spectrum (open symbols in Fig. 6(a)) than the kinetics data employed by Vogler et al. [18]. In addition, as can be seen in Fig. 6(b), the simulation based on the H_2 oxidation kinetics data of Ref. [19] (dashed curve in Fig. 6(b)) is also in reasonable agreement with the present experimental results (open symbols in Fig. 6(b)). The good agreement achieved with the data set reported in Ref. [19] is not completely unexpected, as it has been derived from experimental measurements of Raz et al. [15], which – apart from the present study – is to the best of our knowledge the only experimental work so far, which specifically has focused on the elucidation of the water adsorption/chemisorption and desorption kinetics on YSZ. Although, the thermogravimetry (TG) data presented in the latter work is largely dominated by contributions due to physisorbed water, a detailed numerical simulations of the TG curves reported in Fig. 17 of Ref. [15], which were performed by Goodwin et al. [19], resulted in a reaction kinetics data set, which obviously describes the actual water formation and chemisorptions dynamics on YSZ reasonably well. With a slight adjustment of the kinetics parameters – resulting in the refined surface reaction kinetics data set given in Table I – almost perfect agreement with the experimental TPD data could be obtained.

However, as has been demonstrated in the present work as well as by the earlier work of Wagner [36] the dissociative adsorption of water on YSZ results in a noticeable H_2O dissolution in the YSZ bulk, either as interstitial protons (hydrogen) or interstitial OH, the dynamics of which has not yet been included into the detailed chemical mechanisms employed in computational studies of the electrochemical H_2 oxidation on Ni-pattern/YSZ model anodes although details about an estimate of the current density an interstitial proton transport mechanism through the YSZ bulk might support was given by Mogensen et al. [12]. In addition, the present experimental results on H_2 oxidation and H_2O chemisorptions and dissociation along with the results of the DFT studies of H_2 interaction with YSZ and YSZ + O model surfaces clearly demonstrate the important role the chemical state of the electrolyte surface (oxygen poor versus oxygen rich) plays both in the heterogeneous H_2 oxidation and H_2O dissociation kinetics. In agreement with previous DFT studies [23] the present results emphasize the influence the external oxygen atom supply – either by dissociative adsorption of gaseous O_2 or via bulk oxygen atoms – has on the surface reactivity. Under conditions where external oxygen supply maintains the surface in an oxygen rich (YSZ + O) state the electrolyte surface will be largely hydroxylated with the direct formation of H_2O being the energetically as well as thermodynamically favored H_2 fuel oxidation process. Under these conditions the interaction of gaseous H_2O with the electrolyte will result if the temperature is low enough – as previously proposed by Raz et al. [15] – in the formation of molecular water physisorbed on the hydroxylated electrolyte surface. Under surface oxygen depleting operating conditions, on the other hand, the resulting YSZ surface is virtually inert toward H_2 oxidation and water adsorption followed by dissociation will become the dominating process. Hence, it seems not unreasonable to anticipate that the electrode polarization (anodic versus cathodic) could have a pronounced influence on the actual surface reactivity of the electrolyte. A fact that in conclusion points towards the need of developing more flexible and advanced mathematical sub-models for the description of such polarization induced surface reactivity changes, which, after being included into appropriate reaction diffusion mechanisms might contribute finally to a more detailed understanding and to a consistent theoretical description of not only some selected data but all reliable electrochemical experimental data [8].

Acknowledgements

H.-R. Volpp thanks the German Research Foundation (DFG) for financial support of the experimental work under grant number VO 642/2-1. V. Yurkiv and A. Gorski would like to thank the International Graduate College (IGK 710) "Complex Processes: Modeling, Simulation and Optimization" at the University of Heidelberg for fellowships. Thanks are due to A. Utz (University of Karlsruhe) for providing the YSZ samples used in the present experiments and W. Bessler and M. Vogler (DLR, Stuttgart) for stimulating discussions. M. Shishkin (University of Calgary) is thanked for helpful communications.

References

[1] S.C. Singhal, Solid State Ionics 135 (2000) 305–313.
[2] A. Atkinson, S. Barnett, R.J. Gorte, J.T.S. Irvine, A.J. Mcevoy, M. Mogensen, S.C. Singhal, J. Vohs, Nature Mater. 3 (2004) 17–27.
[3] F. He, D. Song, R.R. Peng, G.Y. Meng, S.F. Yang, J. Power Sources 195 (2010) 3359–3364.
[4] C.W. Sun, U. Stimming, J. Power Sources 171 (2007) 247–260.
[5] R.E. Williford, L.A. Chick, Surface Science 547 (2003) 421–437.
[6] M. Mogensen, J. Høgh, K.V. Hansen, T. Jacobsen, ECS Trans. 1 (2007) 1329–1338.
[7] M. Ihara, T. Kusano, C. Yokoyama, J. Electrochem. Soc. 148 (2001) A209–A219.
[8] S.P. Jiang, S.P.S. Badwal, J. Electrochem. Soc. 144 (1997) 3777–3784.
[9] S.P. Jiang, S.P.S. Badwal, Solid State Ionics 123 (1999) 209–224.
[10] N.Q. Minh, J. Am. Cer. Soc. 76 (1993) 563–588.

[11] S. Primdahl, Ph.D. Thesis, Riso-R-1137(EN), Riso National Laboratory, Roskilde, Denmark, 1999.
[12] M. Mogensen, S. Sunde, S. Primdahl, Proc. 17th Riso Internat. Sym. Mat. Sci. (1996).
[13] P. Holtappels, L.G.J. de Haart, U. Stimming, J. Electrochem. Soc. 146 (1999) 1620–1625.
[14] N. Sakai, K. Yamaji, Y.P. Xiong, H. Kishimoto, T. Horita, H. Yokokawa, J. Electrocer. 13 (2004) 677–682.
[15] S. Raz, K. Sasaki, J. Maier, I. Riess, Solid State Ionics 143 (2001) 181–204.
[16] A. Bieberle, L.P. Meier, L.J. Gauckler, J. Electrochem. Soc. 148 (2001) A646–A656.
[17] A. Bieberle, L.J. Gauckler, Solid State Ionics 146 (2002) 23–41.
[18] M. Vogler, A. Bieberle-Hutter, L. Gauckler, J. Warnatz, W.G. Bessler, J. Electrochem. Soc. 156 (2009) B663–B672.
[19] D.G. Goodwin, H.Y. Zhu, A.M. Colclasure, R.J. Kee, J. Electrochem. Soc. 156 (2009) B1004–B1021.
[20] J. Mizusaki, H. Tagawa, T. Saito, T. Yamamura, K. Kamitani, K. Hirano, S. Ehara, T. Takagi, T. Hikita, M. Ippommatsu, S. Nakagawa, K. Hashimoto, Solid State Ionics 70 (1994) 52–58.
[21] J. Mizusaki, H. Tagawa, K. Isobe, M. Tajika, I. Koshiro, H. Maruyama, K. Hirano, J. Electrochem. Soc. 141 (1994) 1674–1683.
[22] A. Tilocca, A. Selloni, J. Chem. Phys. 119 (2003) 7445–7450.
[23] M. Shishkin, T. Ziegler, J. Phys. Chem. C 112 (2008) 19662–19669.
[24] V. Yurkiv, W.G. Bessler, H.-R. Volpp, 9th European Solid Oxide Fuel Cell Forum, Lucerne, Switzerland, 2010, 9, pp. 1–14.
[25] O.R. Inderwildi, D. Starukhin, H.-R. Volpp, D. Lebiedz, J. Warnatz, in Quantum Chemical Calculations of Surfaces and Interfaces of Materials, American Scientific Publishers, 2009.
[26] M.D. Segall, P.J.D. Lindan, M.J. Probert, C.J. Pickard, P.J. Hasnip, S.J. Clark, M.C. Payne, J. Phys. Condens. Matter 14 (2002) 2717–2744.
[27] J.P. Perdew, J.A. Chevary, S.H. Vosko, K.A. Jackson, M.R. Pederson, D.J. Singh, C. Fiolhais, Phys. Rev. B 46 (1992) 6671–6687.
[28] D. Vanderbilt, Phys. Rev. B 41 (1990) 7892–7895.
[29] H.J. Monkhorst, J.D. Pack, Phys. Rev. B 13 (1976) 5188–5192.
[30] N. Govind, M. Petersen, G. Fitzgerald, D. King-Smith, J. Andzelm, Comp. Mat. Sci. 28 (2003) 250–258.
[31] G. Stapper, M. Bernasconi, N. Nicoloso, M. Parrinello, Phys. Rev. B 59 (1999) 797–810.
[32] X. Xia, R. Oldman, R. Catlow, Chem. Mat. 21 (2009) 3576–3585.
[33] G. Ertl, M. Neumann, K.M. Streit, Surface Science 64 (1977) 393–410.
[34] M.A. Mangan, B.G. Lindsay, R.F. Stebbings, J. Phys. B—Atomic Molecular and Optical Phys. 33 (2000) 3225–3234.
[35] H.C. Straub, B.G. Lindsay, K.A. Smith, R.F. Stebbings, J. Chem. Phys. 108 (1998) 109–116.
[36] C. Wagner, Berichte der Bunsengesellschaft 72 (1968) 778–781.
[37] O. Deutschmann, S. Tischer, S. Kleditzsch, V.M. Janardhanan, C. Correa, D. Chatterjee, N. Mladenov, H.D. Mihn, DETCHEM Software Package, 2.1 ed., Karlsruhe, 2007, www.detchem.com.
[38] A. Hofmann, S.J. Clark, M. Oppel, I. Hahndorf, Physical Chemistry Chem. Phys. 4 (2002) 3500.